Sensors & Actuators: B. Chemical 313 (2020) 127965

Contents lists available at ScienceDirect

Sensors and Actuators B: Chemical

journal homepage: www.elsevier.com/locate/snb

Acetone sensors with high stability to humidity changes based on Ru-doped NiO flower-like microspheres

Man Yang[a], Jingyuan Lu[a], Xi Wang[a], Hong Zhang[a], Fang Chen[a], Jianbo Sun[b], Jiaqi Yang[a], Yanfeng Sun[a,*], Geyu Lu[a,*]

[a] State Key Laboratory of Integrated Optoelectronics, College of Electronic Science and Engineering, Jilin University, 2699 Qianjin Street, Changchun 130012, People's Republic of China

[b] The Key Laboratory for Photonic and Electronic Bandgap Materials, Ministry of Education, School of Physics and Electronic Engineering, Harbin Normal University, Harbin 10025, People's Republic of China

ARTICLE INFO

Keywords:
Ru-doped NiO
Flower-like microspheres
Gas sensor
Acetone
Humidity

ABSTRACT

Humidity dependence of gas sensors is one of the main obstacles for practical application. Through Ru doping into NiO flower-like microspheres, which are synthesized by a one-step hydrothermal route, the gas sensors exhibit high stability to humidity changes. The sensors based on 0.5 at% Ru-doped NiO have almost the same responses to 100 ppm acetone at 200 °C when the relative humidity ranges from 15 % to 90 %. At the same time, they possess the highest response (~12 to 100 ppm acetone), which is about 9 times higher than that based on pure NiO. In addition, the sensors based on 0.5 at% Ru doped NiO sample show good selectivity and good long-term stability. Gas sensing mechanism for the enhanced gas sensing performance is also discussed. The results demonstrate that doping Ru into NiO flower-like microspheres is a promising way for designing high performance acetone gas sensors.

1. Introduction

Nowadays, gas sensors based on metal oxide semiconductor (MOS) have been applied in a broad range of application, including toxic and explosive gas detection, medical diagnosis, food and military security owing to their outstanding merits of moderate price, reliability, low power consumption and simplicity of operation [1–3]. Although the gas sensors based on MOS have many outstanding advantages, the influence of humidity on the response of the gas sensors based on MOS is still a great challenge for further expansion of the application field.

N-type MOS gas sensors have gained much attention because they have high response, short response time and reliable detection to some typical volatile organic gases, such as acetone, ethanol, toluene, and formaldehyde etc. The representative n-type MOS are SnO_2, In_2O_3, ZnO, WO_3 and Fe_2O_3 [4–8]. However, the significant humidity interference limits them for broad gas detection. Pointing to this issue, Zhu et al. have fabricated Pt modified In_2O_3 nanofiber gas sensor and the response to acetone decreases about 30 % when the relative humidity (RH) changes from 25 % to 85 % [5]. Yuan et al. have synthesized Au-Sn doped ZnO through hydrothermal method and reduces the impact of humidity by catalytic effect of noble metal [9]. Material with little dependence on humidity of p-type $La_{0.7}Sr_{0.3}FeO_3$ is used by Li et al. to improve the humidity dependence of In_2O_3-SnO_2 gas sensors [10]. The sensors still show obvious response deterioration with increase of RH even though the humidity influence has been reduced. Lee and Barson et al. have fabricated excellent gas sensors with stability to humidity changes through doping p-type NiO into SnO_2 spheres, and the response and resistance of the gas sensor almost unchanged in dry and 25 % RH air respectively [11]. They demonstrate that NiO can act as a strong humidity absorber and protect SnO_2 from the influence of humidity. However, the work lacks the data about the sensing properties at different RH. The statement above implies that noble metal doping or p-type MOS protection can reduce the influence of humidity on n-type MOS sensor to some extent. However, gas sensors with high stability to humidity changes using gas sensing materials rather than n-type MOS is still desirable.

Fortunately, p-type MOS gas sensors, which possess the distinctive oxygen adsorption properties, can be used to design enhanced performance gas sensors that exhibit high stability to humidity changes and fast recovery properties [12]. Lee has pointed out that the gas response of p-type MOS is equal to the square root of n-type MOS when the morphology and size of both sensing materials are identical [13], which leads to the less publications about p-type MOS gas sensors [12]. Thus, improving the gas response of the gas sensors based on p-type MOS is

* Corresponding authors.
E-mail addresses: syf@jlu.edu.cn (Y. Sun), lugy@jlu.edu.cn (G. Lu).

https://doi.org/10.1016/j.snb.2020.127965
Received 21 October 2019; Received in revised form 6 March 2020; Accepted 9 March 2020
Available online 10 March 2020
0925-4005/

necessary. Nickel oxide (NiO), as a typical p-type MOS, has drawn extensive attention due to their wide band gap (Eg = 3.6–4.0 eV), large specific areas, eminent structural stability, excellent transportation properties and high oxygen adsorption capacity [14–17]. However, pristine NiO without effective modification shows a low response to tested gases when used in gas sensors as a sensing material [18,19]. Therefore, it is necessary to improve the sensitivity of the gas sensors based on NiO materials. Sol-gel method has been used to synthesize NiO particles doped with foreign metal [20,21]. However, the increase of response is less than 3 times using this synthesis procedure, which might be due to the agglomeration of nanoparticles and low utility factor of the sensing body. Spray pyrolysis method has the same problem as Sol-gel method [22]. Through adding dextrin in the precursor solution and forming the multiroom structure, the response of the gas sensors based on Sn-doped NiO towards p-xylene can be increased about 9 times, which verifies that morphology has great influence for the gas sensing properties [23]. Hydrothermal method can not only control the particles size, but also adjust the morphology of the synthesized material via changing the types of surfactants, pH value, synthetic temperature, solution environment, salt concentration and so on [24–27]. Through doping foreign metal, the response of the gas sensor can be enhanced far more than 3 times. As for the researches about humidity influence on gas sensing properties, Zhu et al. have synthesized Al doped NiO porous nanowires and investigated the humidity effect on gas response [24]. They find that the sensors have the highest response at 45 % RH due to less exposure of hydroxyl group. The sensors based on Zn-doped NiO are fabricated by Fomekong et al., and the baseline resistance will increase greatly with the increase of RH [28]. Might be inspired by Kim's work [11], Gao et al. have synthesized Sn doped NiO microspheres and the gas sensors based on the 1.5 at% Sn^{2+}-NiO sample exhibit excellent humidity-independent performance [29]. They ascribe the humidity-independent phenomenon to the defect-rich surface of the sensing material. Therefore, it is still meaningful and desirable to develop gas sensors with excellent gas sensing performance and high stability to humidity changes based on NiO material.

On the basis of above, humidity interference is one of the key issues for the practical application of gas sensors based on MOS. The main purpose of this work is to fabricate NiO based gas sensors with improved gas response and high stability to humidity changes. In this work, hydrothermal method is used to fabricate flower-like NiO microspheres. Moreover, Ru is chosen as dopant in NiO to enhance the gas sensing performance of NiO-based gas sensors. The comparative sensing property testes show that the sensor based on 0.5 at% Ru-doped NiO has the highest gas response, good selectivity and high stability to humidity changes to the target gas of acetone, demonstrating that suitable amount of Ru doping into NiO material has potential application for a superior acetone gas sensor.

2. Experimental section

2.1. Synthesis of pure and Ru-doped NiO flower-like microspheres

All the relevant chemicals were of analytical grade and used directly without purification. Pure NiO flower-like microspheres were synthesized utilizing a hydrothermal method. Typically, 1.163 g Nickel nitrate hexahydrate ($Ni(NO_3)_2.6H_2O$) and 0.782 g Cetyltrimethyl Ammonium Bromide (CTAB) were dissolved in a mixed solution which contained 23 ml deionized (DI) water and 23 ml 1,2-propanediol. Next, 0.2 g urea and 0.2 g polyethylene glycol (PEG-2000) were added in the above solution with continuous stirring. After 30 min at room temperature, the mixed solution was then transferred into a 100 ml autoclave and reacted at a fixed temperature of 180 °C for 24 h. After that, the products were collected and rinsed several times using deionized (DI) water and ethanol alternately for three times. Finally, the precipitates were dried at 80 °C for 24 h and annealed at 600 °C for 4 h in a muffle with a heating rate of 2 °C/min. The synthesis of Ru-doped NiO flower-like microspheres was similar to the above process. A little bit difference was that vary amounts of (0.004 mmol, 0.02 mmol, 0.04 mmol, 0.06 mmol) Ruthenium trichloride ($RuCl_3.xH_2O$) were added in the reaction mixture after adding $Ni(NO_3)_2.6H_2O$ and CTAB. The ratio of Ru/Ni was set at 0, 0.1 at%, 0.5 at%, 1 at% and 1.5 at%, respectively.

2.2. Characterization

The phase and crystalline information of pure and Ru-doped samples was collected with the help of the X-ray powder diffraction (XRD) analysis using a Rigaku D/Max X-ray diffractometer with Cu Ka radiation, which was operated at 40 kV and 200 mA in the 2θ range from 20° to 80°. The scanning step size and speed were 0.02° and 10° min^{-1}, respectively. To better resolve the peak shifts, a reduced scanning step size (0.0184°) and speed (1° min^{-1}) were applied. The microstructures and size of the as-prepared materials were characterized by field emission scanning electron microscopy (FESEM) using a JSM-700 F (JEOL) microscope, transmission electron microscopy (TEM) and high-resolution transmission electron microscopy (HRTEM) using a JEM-2200FS (JEOL). The energy-dispersive X-ray spectroscopy (EDS) images were obtained on the TEM attachment. The X-ray photoelectron spectroscopy (XPS) investigations were carried out with the source of Mg Kα X-ray (1253.6 eV Specs XR50).

2.3. Fabrication and measurement of gas sensor

The schematic diagram of the fabricated gas sensor is shown in Fig. 1a and the fabrication process of a gas sensor can be roughly divided into four steps: Firstly, the as-synthesized powder was mixed with ethanol to get a uniform slurry. After that, the slurry was coated on an alumina tube (external diameter: 1.2 mm, internal diameter: 0.8 mm, length: 4 mm) using little clean brushes. Then, the coated ceramic tube was sintered at a constant temperature of 300 °C for 3 h in a muffle furnace. Thirdly, a Ni-Cr alloy was installed through the tube providing different heating temperatures via the variation of flowing current. Finally, the resulting device was welded on a hexagon socket. Gas sensing properties were investigated through a static test system (Fig. 1b) after aging the well-fabricated sensing device for five days with an aging current of 90 mA at the laboratory conditions (20 °C, 50 % RH). The humidity influence was tested using the programmable temp. & humi. test chamber. Gas response (S) is defined as the ratio of the stable resistance of the sensor in target gases (R_g) and the stable resistance in air (R_a). Respectively, the response and recovery time is defined as the time required to achieve 90 % of the variation in resistance after the sensor is in target gases and air.

3. Results and discussion

3.1. Structural and morphological characteristics

XRD patterns of pure and Ru-doped NiO powders are presented in Fig. 2a. It is clearly that all the diffraction peaks of all the samples are matched well with the face-centered cubic NiO (JCPDS NO.44-1159). And no other diffraction peaks related to Ru compound or any impurities appear in the patterns of 0.1–1.5 at% Ru-doped NiO samples. Fig. 2b displays the patterns of the high-resolution (200) and (220) peaks of pure and Ru-doped NiO samples. Obviously, there is a small shift towards a higher angle in the Ru-doped NiO samples, and the shift becomes larger with the increase of Ru doping amount, which indicates the successful incorporation of Ru into the NiO lattice. This behavior can be attributed to the radii of 6-coordinate Ru^{3+} ions (0.068 nm) [30] are smaller than that of Ni^{2+} (0.069 nm) [23]. Additionally, the detailed crystallite sizes of pure, 0.1 at%, 0.5 at%, 1 at% and 1.5 at% Ru-doped NiO samples are about 31.9 nm, 28.6 nm, 26.7 nm, 25.6 nm and 23.7 nm, calculated by Scherrer formula ($D = 0.89\lambda/\beta\cos\theta$), where λ is the X-ray wavelength and β is the peak width at half height. It is clear

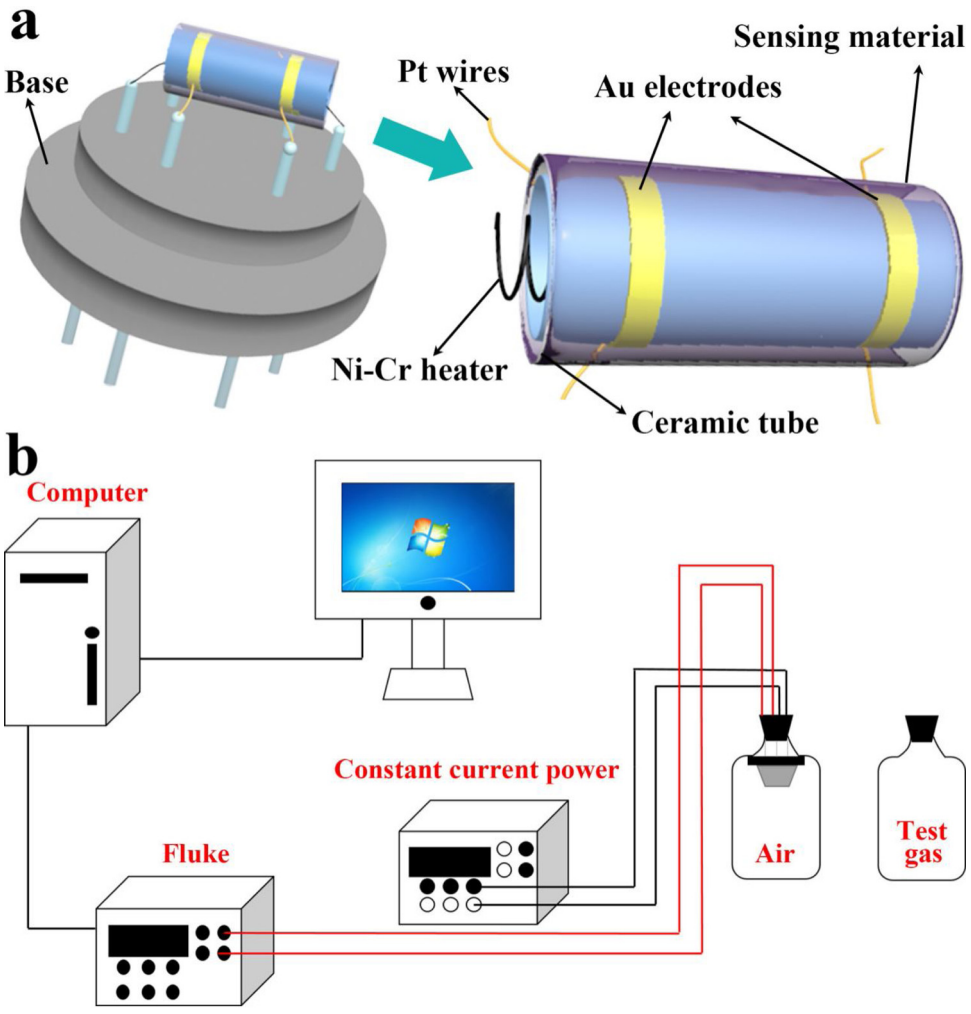

Fig. 1. Schematic diagram of the **(a)** gas sensor **(b)** static test system.

that the crystallite size decreases with the increase of Ru doping amount. In addition, the changes of crystallite size can reflect changes in grain(particle) size in some way. And according to the previous reports, reducing particle size improves sensitivity [31]. The morphologies of pure and Ru-doped NiO samples examined by SEM are shown in Fig. 3a–e, respectively. It can be found that pure NiO sample exhibits the flower-like microspheres morphology composed of interweaved nanosheets with good uniformity and dispersion (Fig. 3a). When only a small amount of Ru (0.1 at%) is doped into the sample, no obvious morphology change can be detected (Fig. 3b). When the doping amount of Ru reaches to 0.5 at%, the petals of the flower-like microspheres become thinner and denser (Fig. 3c). With the Ru doping amount reaching to 1 at%, the flower-like microspheres tend to coagulate (Fig. 3d). The flower-like morphology will be broken into nanoparticles with further increase of the Ru doping amount to 1.5 at%. SEM images containing a single microsphere of pure and Ru-doped NiO powders are displayed in Fig. 3f–i. The insets of Fig. 3f–i show part of the nanosheets corresponding to each microsphere. It is obvious that the petals of flower-like microspheres with some small holes on them are consisted of many nanoparticles. TEM and HRTEM are employed to further observe the structure information of the pure and 0.5 at% Ru-doped NiO samples (Fig. 4a–f). As shown in Fig. 4a and d, the size and morphology

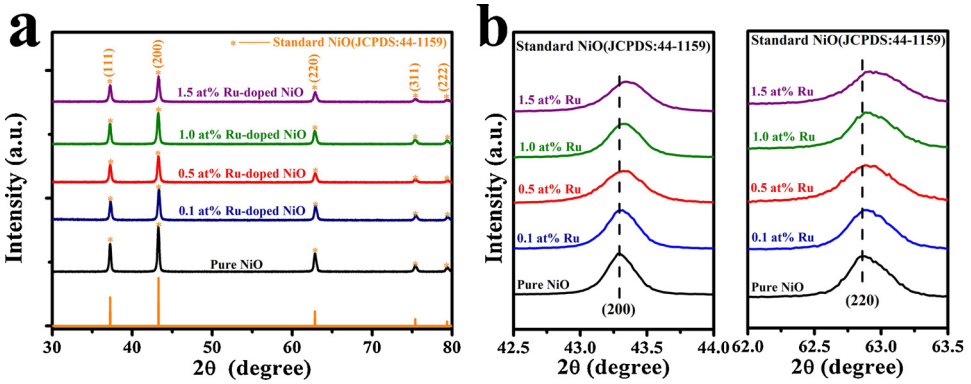

Fig. 2. (a) XRD patterns and **(b)** high resolution of (200) and (220) peaks of pure, 0.1 at%, 0.5 at%, 1.0 at%, 1.5 at% Ru-doped NiO flower-like microspheres.

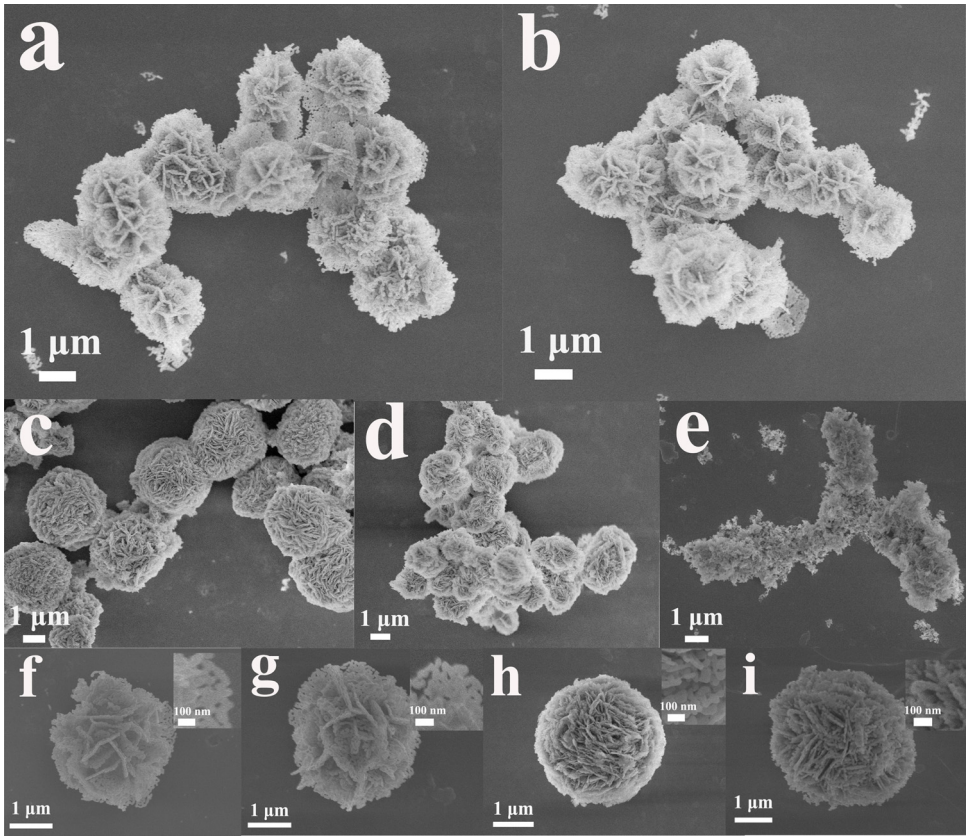

Fig. 3. (a–e) SEM images of pure, 0.1 at%, 0.5 at%, 1.0 at%, 1.5 at% Ru-doped NiO flower-like microspheres. **(f-i)** SEM images of single flower-like microsphere of pure, 0.1 at%, 0.5 at%, 1.0 at% Ru-doped NiO.

of the pure and 0.5 at% Ru-doped NiO match well with the results of the SEM images. High magnification images of pure and 0.5 at% Ru-doped NiO are displayed in Fig. 4b and e. The rectangle marked areas demonstrate the nanosheets of flower-like microspheres are 2D networks consists of many nanoparticles. HRTEM images of the pure and 0.5 at% Ru-doped NiO samples are displayed in Fig. 4c and f, from which clear lattice fringes with 0.147 nm and 0.127 nm can be clearly observed, corresponding to (110) and (113) lattice planes of cubic NiO. Fig. 4g–j provide the element mappings of the single microsphere. Obviously, all the elements (Ni, O and Ru) are detected and distributed uniformly along the shape of the flower-like microsphere. Besides, the element mappings with higher magnification also have been tested (shown in Fig. 4k-n), due to the limitation of the spatial resolution and the element content resolution, when element mappings are magnified to the extent of Fig. 4k–n, the signal of the edge along the shape of flower-like microsphere becomes weaker. But it can also be founded that the signal of Ru is much weaker than that of Ni, indicting the small proportion of Ru doping into NiO sample.

XPS measurement was adopted to analyze the surface or near-surface chemical compositions of all the samples. Fig. 5a is the survey scan of pure and 0.5 at% Ru-doped NiO samples. The Ru 3d XPS spectrum of 0.5 at% Ru-doped NiO is displayed in Fig. 5b. In detail, the peak located at 282.1 eV can be assigned to Ru^{3+} $3d_{5/2}$, indicating the Ru doping in NiO crystals [23,32,33]. The high resolution survey scans of Ni 2p are shown in Fig. 5c–d, in which the peaks present at 855.4 eV can be assigned to Ni $2p_{2/3}$ [34]. As shown in Fig. 5g–i, the peaks of O 1s are asymmetric and can be fitted into lattice oxygen (O_L), deficient oxygen (O_D)and chemisorbed oxygen (O_C) with binding energy about 529.3 ± 0.6 eV, 530.1 ± 0.4 eV and 532.4 ± 0.3 eV, respectively [35,36], which is discussed in detail in gas mechanism section. Since halogen contents are also important in the general performance of catalytic material, the bromine content was also checked by the XPS measurement. The obtained XPS data shows that the content of bromine in 0.5 at% Ru-doped NiO sample is about 0.7 at%. But we mainly study the impact of Ru doping on the gas sensing performance in this paper, the impact of bromine content will be studied in the next work.

The N_2 adsorption/desorption and pore size distribution isotherms of pure NiO and 0.1–1.5 at% Ru doped NiO are displayed in Fig. 6a–e. The textural parameters of all the samples from BET analysis are summarized in Table 1. Clearly, with the increase of the Ru doping amount, the specific surface areas become higher. The higher specific surface areas can provide more active sites so as to enhance the gas sensing performance. Moreover, 0.5 at% Ru-doped NiO sample shows largest pore volume and average pore size, which are almost three and two times than that of pure NiO sample, respectively. Thus, the utility factor of the sensing body will increase, leading to the enhancement of gas response.

3.2. Gas sensing characteristics

All the sensing performance tests (except for the humid interference test) were collected under a laboratory conditions (50 % RH, 20 °C), which was controlled and maintained by a big air conditioner. The working temperature is an important factor for gas sensing performance, and can affect carrier concentration of the sensing body, gas adsorption and desorption processes of the gas molecules [36]. Hence, the relationship between gas sensitivity to 100 ppm acetone and working temperature of the sensors based on pure and 0.1 at%-1.5 at% Ru-doped NiO samples under the laboratory conditions is shown in Fig. 7a. Clearly, the response-working temperature curves present volcanic shapes. Meanwhile, the optimal operating temperatures for the 0.1–1.5 at% Ru-doped NiO samples are 200 °C, and for the pure NiO sample is 225 °C, demonstrating the decrease of optimal operating temperature because of Ru doping. Furthermore, the gas response of the

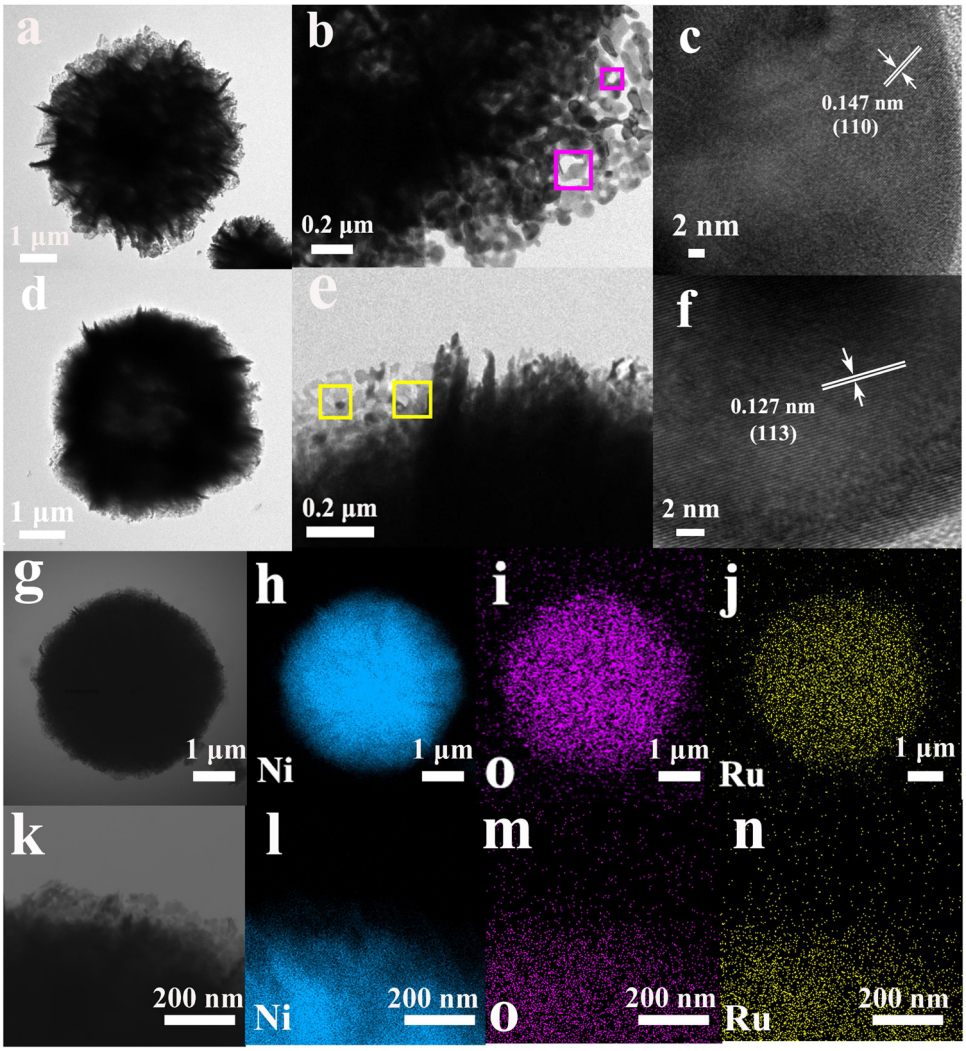

Fig. 4. (a, b) Typical Tem images and **(c)** HRTEM of pure NiO. **(d, e)** Typical Tem images and **(f)** HRTEM of 0.5 at% Ru-doped NiO. **(g–j)** Scanning TEM (STEM) images and corresponding elemental mapping images of 0.5 at% Ru-doped NiO sample. **(k–n)** Scanning TEM (STEM) images and corresponding elemental mapping image of 0.5 at% Ru-doped NiO sample with higher magnification.

gas sensors based on the pure, 0.1 at%, 0.5 at%, 1 at% and 1.5 at% Ru-doped NiO samples to 100 ppm acetone at their optimal operating temperature is 1.3, 3.0, 12.6, 7.4 and 6.8, respectively. Obviously, the sensor based on 0.5 at% Ru-doped NiO sample possesses the highest gas response to 100 ppm acetone (12.6), which is about 9.6 times higher than that based on pure NiO sample. It demonstrates that Ru doping is an effective way to improve the gas response of the sensors based on NiO material towards acetone.

Given that selectivity plays an important role for gas sensors in the practical use [37], the response of the gas sensors based on pure and all Ru-doped NiO samples to 100 ppm different target gases (acetone, ethanol, methanol, formaldehyde and benzene) were investigated and the results are shown in Fig. 7b. It is clear the Ru doping can obviously increase the gas responses to all of the tested gases. Besides, all the sensors show higher responses to acetone compared with other interfering gases. Among them, the gas sensor based on 0.5 at% Ru-doped NiO shows the highest response to 100 ppm acetone and about 1.8–6.3 times as high as that of other target gases, but the ratio of the sensor based on pure NiO is only about 1.03–1.17, indicating the improved selectivity property to acetone through Ru doping. To better reflect the selectivity of the sensor, the cross-selectivity is defined as the ratio between the response values to target gas and that to the highest interfering gas [38–40]. The responses to 100 ppm acetone and 100 ppm ethanol at different operating temperature are shown in Fig. 7c. Significantly, the response to acetone is higher than that to ethanol all the time at the wide temperature range. And the cross-selectivity is analyzed and plotted in Fig. 7d. Clearly, the selectivity to acetone is about 2 times towards ethanol at 200 °C, the selectivity value is quite good for metal oxide-based sensors [41].

Fig. 7e displays the dynamic sensing transients of the sensors based on pure and 0.5 at% Ru-doped NiO samples to 5 – 500 ppm acetone at their optimal operating temperature. It shows that the responses of both sensors increase in steps with the increase of the gas concentrations, and the responses of 0.5 at% Ru-doped NiO-based sensor are higher than that of pure NiO-based sensor to the different concentrations of acetone gases. In addition, both sensors exhibit good response/recovery properties and reversible performances. The responses of both sensors as a function of different acetone concentrations at their respective optimal operating temperature are shown in Fig. 7f. It can be found the response of 0.5 at% Ru-doped NiO-based sensor shows a rapid increase at low acetone concentration (from 5 ppm to 70 ppm). Then the responses increase slowly when the sensor is exposed to high concentration of acetone (from 100 ppm to 500 ppm), but the response doesn't tend to saturation. These results indicate that 0.5 at% Ru-doped NiO-based sensor has a wide test range and is a promising candidate for real-time monitoring of acetone gas.

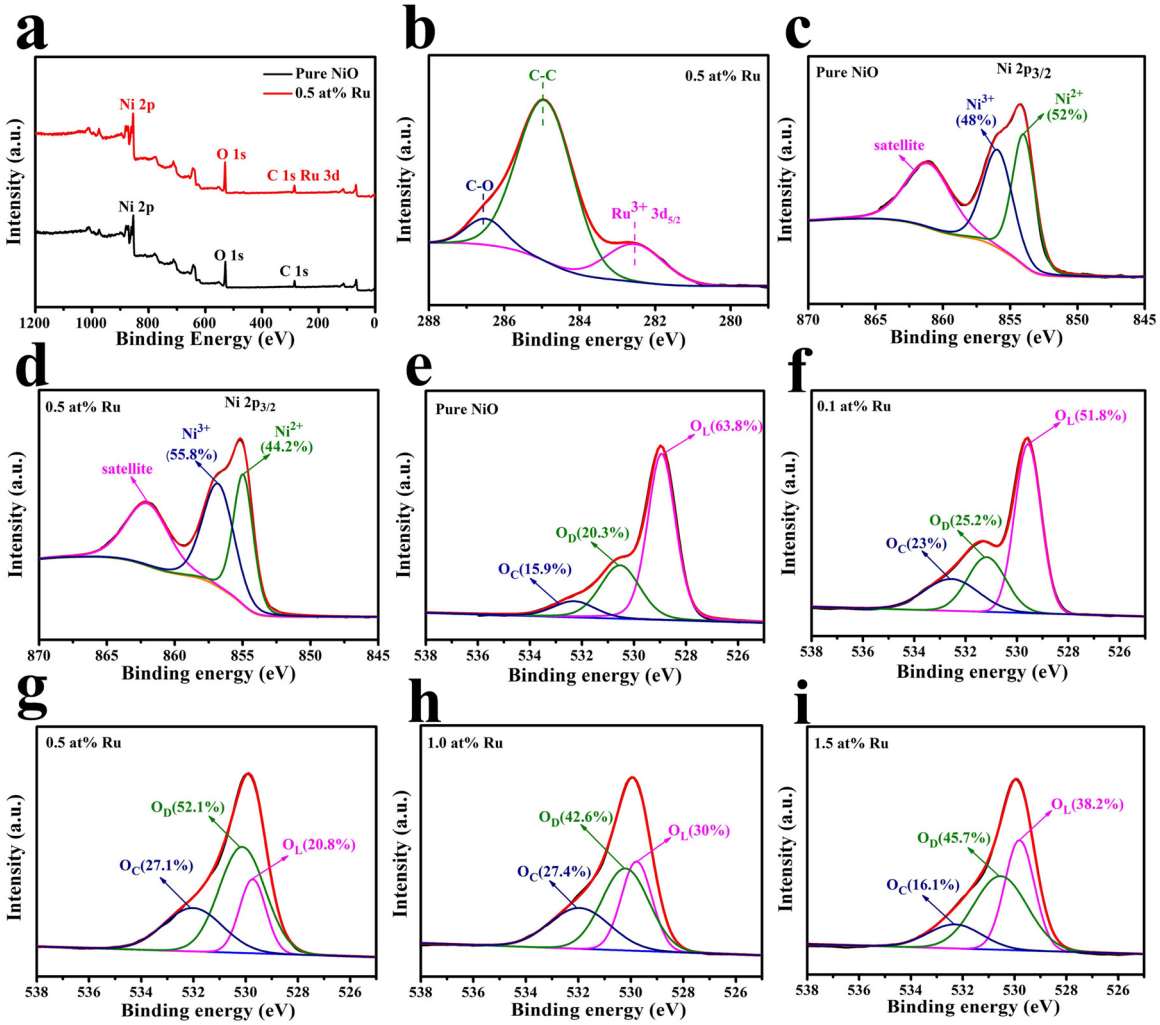

Fig. 5. (a) XPS survey scan **(b)** Ru 3d XPS spectra of 0.5 at% Ru-doped NiO flower-like microspheres. **(c, d)** the high resolution scans of pure and 0.5 at% Ru-doped NiO for Ni $2p_{3/2}$. **(f–g)** O 1s XPS spectra of pure, 0.1 at%, 0.5 at%, 1.0 at%, 1.5 at% Ru-doped NiO flower-like microspheres, respectively.

The four detailed response recovery curves to 100 ppm acetone of the sensor based on 0.5 at% Ru-doped NiO sample at 200 °C are shown in Fig. 8a. It can be discovered that the resistance increase immediately when exposed to 100 ppm acetone, and become saturated quickly. The resistance will go back to previous value when exposed back to air, revealing the typical characteristics of sensors based on p-type MOS. The response and recovery times of the 0.5 at% Ru-doped NiO-based sensor calculated by the four curves are 72 s, 72 s, 70 s, 68 s and 22 s, 25 s, 21 s, 24, respectively. So the average response and recovery time are 71 s and 23 s. Fig. 8b displays five reversible cycles of response and recovery curves to 100 ppm acetone of the sensor based on 0.5 at% Ru-doped NiO sample at 200 °C. Clearly, there are no obvious decrease of the gas responses, which demonstrates the excellent reproducibility and repeatability of the 0.5 at% Ru-doped NiO-based sensor. Fig. 8c displays the initial resistance in air of the sensors based on pure and 0.1–1.5 at% Ru-doped NiO samples at different working temperatures. The resistances of all the sensors decrease with the increase of the working temperature, indicating their semiconductor properties. In addition, the resistances will increase with the increase of Ru content at the same working temperature. The long-term stability test of the sensor based on 0.5 at% Ru-doped NiO sample to 100 ppm acetone was carried out in 14 days and the result is shown in Fig. 8d. It can be seen that the initial resistance and the response just have a slight change in a small range and the average resistance and response is ~1.4 MOhm and 11.6. The result indicates that the 0.5 at% Ru-doped NiO gas sensor has good long-term stability, which is crucial in the practical application.

As humidity is a negative factor to influence the sensing performance of a gas sensor, the corresponding tests were finished to investigate the effects of humidity on gas sensors under different RH. For the humidity test of the sensor, a humidity chamber (Shanghai ESPC Environment Equipment Corporation, China) which worked at a constant temperature (20 °C) was used to provide different humidity atmospheres for the 11 test chamber. The Fig. 9a shows the dynamic response-recovery curves of the 0.5 at% Ru-doped NiO based gas sensor to 100 ppm acetone at 15, 30, 50, 60 and 90 % RH. Clearly, all the real-time resistances of the sensor increase quickly when exposed to 100 ppm acetone, and decrease rapidly back to its original value when exposed to air. The responses of 0.5 at% Ru-doped NiO-based sensor in relation with RH to 100 ppm different target gases (acetone, ethanol, methanol, formaldehyde and benzene) at 200 °C are shown in Fig. 9b. Apparently, the responses to all of these VOC gases are almost unchanged, and the gas sensor still has the highest response to 100 ppm acetone among the tested VOC gases, indicating the stable selectivity under different RH. The response and resistance of 0.5 at% Ru-doped NiO-based sensor to 100 ppm acetone at 200 °C versus various RH are plotted in Fig. 9c. The responses under 15, 30, 50, 60 and 90 % RH are 11.26, 12.35, 12.58, 11.28 and 11.55, respectively. We can see that the change of response and baseline resistance can be ignored under various RH. In brief, humidity has almost no influence on the gas response, baseline resistance, selectivity and response recovery characteristics.

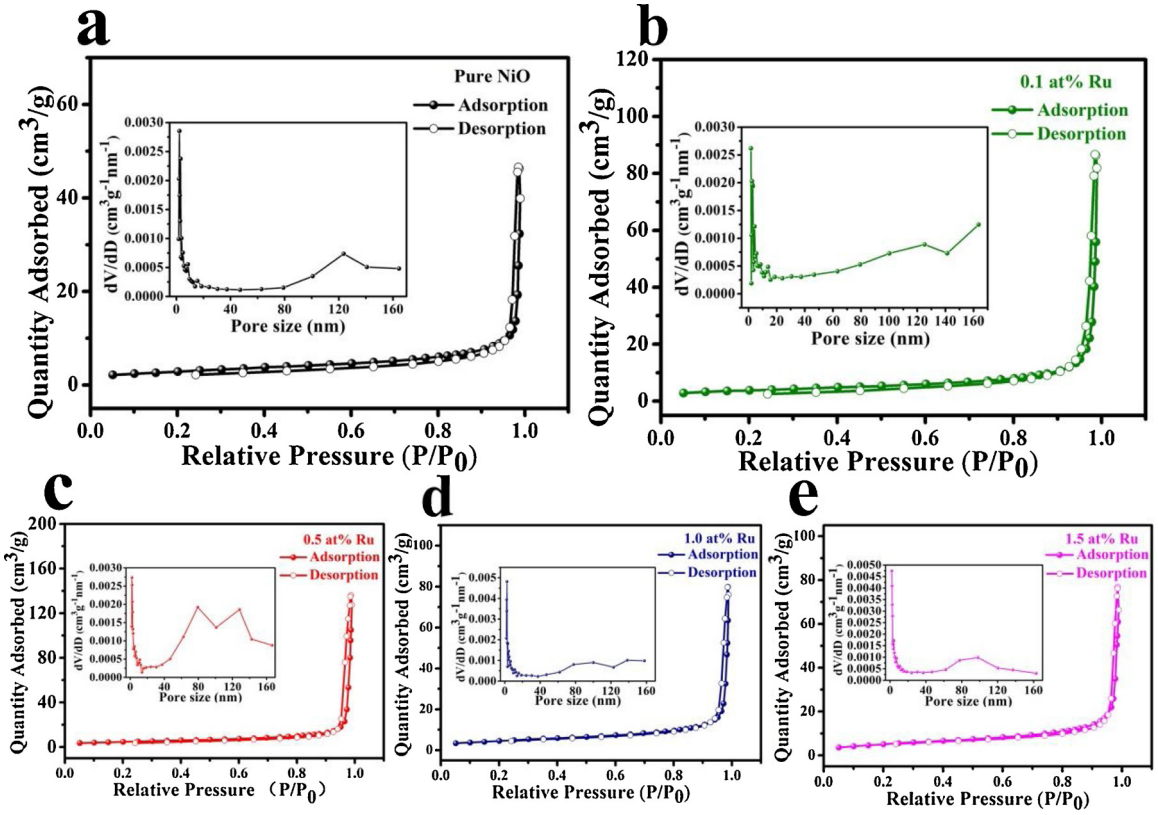

Fig. 6. (a–e) N_2 adsorption and desorption isotherms of pure, 0.1 at%, 0.5 at%, 1.0 at%, 1.5 at% Ru-doped NiO samples, respectively.

Table 1
The textural parameters of all the samples from BET analysis.

Samples	Surface area ($m^2 g^{-1}$)	Pore volume ($cm^3 g^{-1}$)	Average pore size (nm)
Pure NiO	16.40	0.06	23.87
0.1 at% Ru	20.97	0.13	38.37
0.5 at% Ru	26.15	0.20	47.61
1.0 at% Ru	26.51	0.12	28.28
1.5 at% Ru	30.06	0.10	21.98

The sensing performance of the gas sensor in this work and other reported acetone gas sensors [42–51] are compared and shown in Table 3. Apparently, the gas sensor based on our 0.5 at% NiO shows a higher response at a relative low operating temperature. A low operating temperature is beneficial to practical application and is environment-friendly because of energy saving. Furthermore, the ratio of the gas response under a high humidity condition and that under low humidity condition could reflect the influence of humidity to the sensing performance. In this work, the ratio of the gas sensor based on 0.5 at% Ru-doped NiO sample is 0.97, indicating the negligible influence of humidity. Hence, it could be concluded that the gas sensor based on 0.5 at% Ru-doped NiO sample has improved sensing performance with a high response at a low operating temperature, high stability to humidity changes and large improved ratio.

3.3. Gas sensing mechanism

For the MOS resistive gas sensor, the generally accepted sensing mechanism is the change of electrical conductivity caused by the chemical reactions between the surface chemisorbed oxygen species and the target gas [52]. Therefore, it's necessary to investigate the change of carrier concentration and the distribution of oxygen species in the sensing materials. The substitution of Ru^{3+} at the site of Ni^{2+} can be compensated by the two different charge compensation mechanisms: electronic compensation and ionic compensation [53,54]. The two charge compensation mechanisms can be explained as follows:

$$Ru_2O_3 \xrightarrow{NiO} 2Ru_{Ni}^{\bullet} + 2e' + 2O_o^{\times} + \frac{1}{2}O_2(g) \quad (1)$$

$$Ru_2O_3 \xrightarrow{NiO} 2Ru_{Ni}^{\bullet} + 3O_O^{\times} + V_{Ni}'' \quad (2)$$

In the electronic compensation mechanism, the electrons are generated to compensate the substituting of Ru^{3+} into Ni^{2+} site as displayed in Eq. (1), which neutralizes holes in NiO and lead to the increase of R_a. It is consistent with the results as shown in Fig. 8c. If the charge compensation is attributed to the ionic species like V_{Ni}'', the hole concentrations will not change much. Accordingly, the increase of the resistance of sensor by Ru doping suggest the electronic compensation mechanism is more plausible. The Ni^{3+}/Ni^{2+} ratios of the pure NiO and 0.5 at% Ru-doped NiO samples are calculated to be 0.92 and 1.26, respectively (shown in Fig. 5c and d). According to the literatures [55,56], the Ni^{3+} can be formed by negatively charged oxygen on the surface of NiO and/or by the excess of negatively charged interstitial oxygen (O_i''). Therefore, the increase of Ni^{3+} / Ni^{2+} ratio caused by Ru doping can be attributed to the conversion of oxygen molecules generated by the reaction in Eq. (3) into negatively charged oxygen at the surface or inside the lattice, which also indicates the incorporation of Ru^{3+} into the NiO crystals.

$$\frac{1}{2}O_2 + 2NiO \xrightarrow{2NiO} O_{surf}''(orO_i'') + 2Ni_{Ni}^{\bullet} + 2O_O^{\times} \quad (3)$$

The charge carrier concentration of oxide semiconductors in air is a key point for gas response [57]. The gas response can be defined and as shown in Eq. (4), where R_g, R_a and p_g, p_a are the resistances and the hole concentrations of gas sensor in the target gas and in air, and $\Delta p = p_a - p_g$ is the variation of hole concentration exposed to reducing gas [53,58]. Obviously, for the p-type MOS, a higher response can be

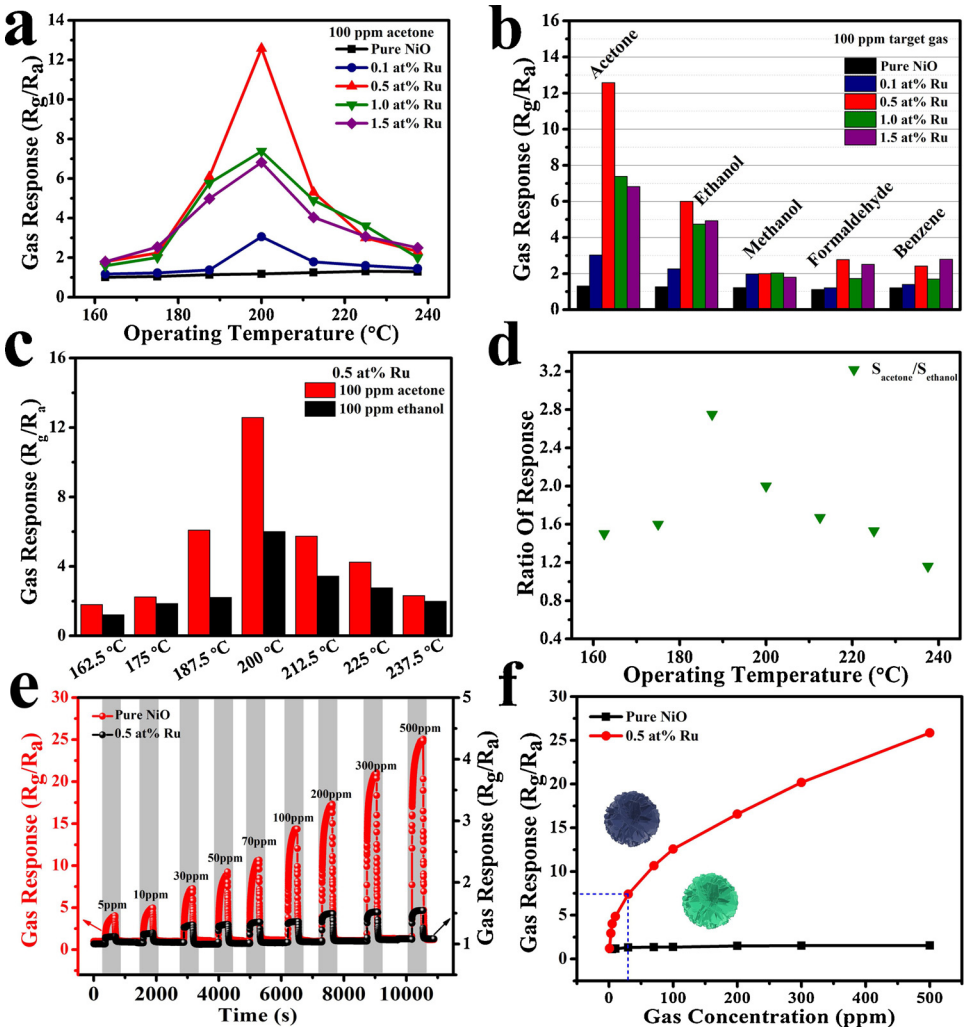

Fig. 7. (a) Gas responses of the sensors based on pure, 0.1 at%, 0.5 at%, 1.0 at%, 1.5 at% Ru-doped NiO samples vs operating temperature exposed to 100 ppm acetone. **(b)** Gas responses of five sensors to 100 ppm various target gases (acetone, ethanol, methanol, formaldehyde, benzene). **(c)** Gas response of the 0.5 at% Ru-doped NiO sensor to 100 ppm acetone and ethanol at various working temperature. **(d)** Relative responses of acetone to ethanol (100 ppm) at various working temperatures. **(e)** Dynamical response curves of the sensors based on pure NiO and 0.5 at% Ru-doped NiO samples. **(f)** Gas response of the sensors based on pure NiO and 0.5 at% Ru-doped NiO samples as a function of the concentration of acetone at 200 °C.

achieved from a lower hole concentration. As shown in the Fig. 10, the Ru replaces the sites of Ni, which can release electrons in the process (shown in eq 1). Therefore, the decrease of the hole concentration can lead to the enhanced gas response due to Ru doping into the NiO crystals.

$$S = \frac{R_a}{R_a} = \frac{p_g}{p_g} = \frac{\Delta p}{p_a - \Delta p} + 1 \quad (4)$$

In addition, the relative percentages of O_L, O_D and O_C in all the samples are summarized in Table 2 obtained from Fig. 5e–i. It could be found the 0.5 at% Ru-doped NiO sample has the highest defect oxygen percentages (52.1 %), which is almost 2.57 times higher than that of pure NiO (20.3 %). The defect oxygen consists of two kinds of oxygen: oxygen vacancies and oxygen interstitials, which can provide more active sites for the gas adsorption and reaction [59,60]. Moreover, the increase of chemisorbed oxygen means more oxygen participate in the gas reaction [61]. Therefore, the sum of defect oxygen and chemisorbed oxygen can reflect the gas properties of the gas sensor. The sum of defect oxygen and chemisorbed oxygen of pure NiO and 0.1–1.5 at% Ru-doped NiO are 36.2 %, 42.8 %, 79.2 %, 70 % and 61.8 %, respectively, which are in agreement with their corresponding gas response. Clearly, the 0.5 at% Ru-doped NiO-based gas sensor shows the highest O_C and O_D sum and the highest gas responses. Thus, the large percentage of defect oxygen and chemisorbed oxygen are thought to be the second reason for the gas response enhancement.

The reasons of enhanced gas sensing performance after doping can be further explained by chemical sensitization mechanism of Ru [62,63]. Ru additive can serve as a catalyst and activates a target gas to facilitate its reaction with adsorbed oxygen on the semiconductor. Thus the additive increases the sensitivity as it increases the rate of the chemical reaction [64]. Furthermore, it is reported that the addition of noble metals can reduce the optimal operating temperature, this behavior arises from the increase in the rate of the target gas oxidation due to the catalysis of the noble metal [65]. Therefore, the decrease of the optimal operating temperature from 225 °C to 200 °C after Ru doping (Fig. 7a) can also verify the catalytic effect of Ru.

As for the high stability to humidity changes of the sensor based on 0.5 at% Ru-doped NiO sample, the defect-rich surface of NiO sample might be the main reason. A water -oxygen reaction can be expressed as follows:

$$O^-_{(ad)} + H_2O_{(gas)} + 2Ni_{Ni} + h^+ \leftrightarrow 2(Ni^+_{Ni} - OH^+) + S \quad (5)$$

In the Eq. (5), $O^-_{(ad)}$ stands for an ionosorbed oxygen species, $H_2O_{(gas)}$ is a water molecule, Ni_{Ni} describes a surface-Ni site, h^+ is consumed hole, S is an active site on the surface for the chemisorption of oxygen and $Ni^+_{Ni} - OH^-$ is the formed terminal hydroxyl group [66]. It can be founded in this formula the water molecule in atmosphere will compete oxygen species with the target gases, which can reduce the gas response. The 0.5 at% Ru-doped NiO is rich in defects and has high percentage of defect oxygen (52.1 %). When in a humid atmosphere, the water molecules will absorb on the site of defects in NiO so that fewer water molecules compete for chemisorbed oxygen with target gases [67,68]. Therefore, the impact of humidity to gas response will be decreased with the defect-rich surface. In addition, the catalytic effect

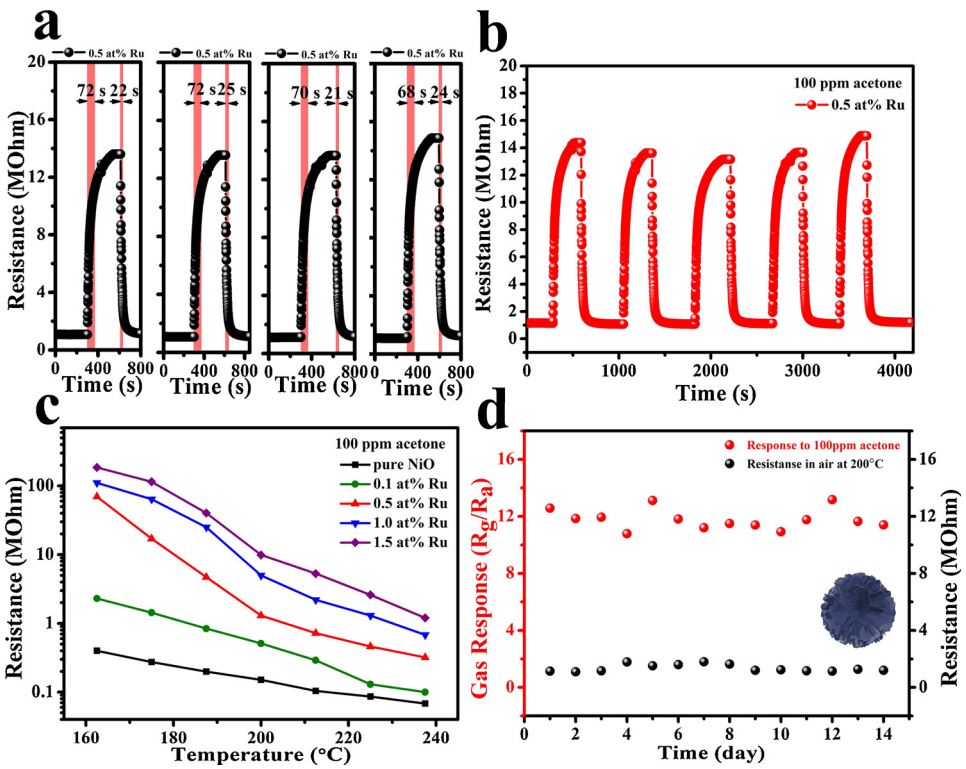

Fig. 8. (a) Four response and recovery characteristics of the sensor based on the 0.5 at% Ru-doped NiO sample to 100 ppm acetone at 200 °C. **(b)** Five dynamic response curves of the 0.5 at% Ru-doped NiO sensor to 100 ppm acetone at 200 °C. **(c)** The dependence of the resistances in air on the doping amount of Ru for the sensors at different temperature. **(d)** Initial resistance and gas response to 100 ppm acetone of the 0.5 at% Ru-doped NiO sensor in the 14-day test at 200 °C.

of Ru is also beneficial for the anti-humidity properties due to the increased surface adsorbed oxygen ions and the catalytic effects on the gas reaction. Both of them will decrease the impact of RH on the resistance and facilitate the gas reaction with the surface of the sensing body. Thus the RH contribution to the total resistance change will be reduced.

4. Conclusions

In summary, pure and Ru-doped (0.1, 0.5, 1.0, 1.5 at%) NiO flower-like microspheres are synthesized through a one-step hydrothermal method. A systematic and comprehensive test of gas sensors fabricated from the above samples reveal that the 0.5 at% Ru-doped NiO-based sensor shows the highest gas response to 100 ppm acetone. Besides, the baseline resistance, gas responses and selectivity of the gas sensor are almost unchanged at different RH ranging from 15 %–90 %. The

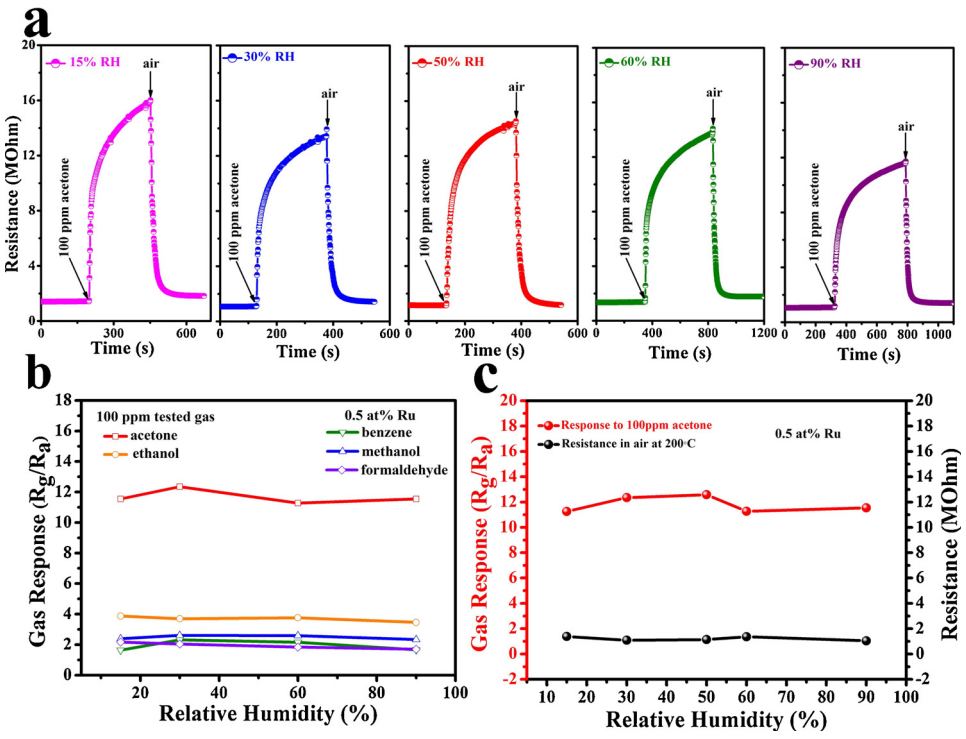

Fig. 9. (a) Dynamic response curves of the 0.5 at% Ru-doped NiO sensor at various humidity (15–90 % RH) at 200 °C. **(b)** Gas response of the 0.5 at% Ru-doped NiO sensor as a function of relative humidity to 100 ppm various target gases (acetone, ethanol, methanol, formaldehyde, benzene) at 200 °C. **(c)** Initial resistance and gas response to 100 ppm acetone of the 0.5 at% Ru-doped NiO sensor as a function of relative humidity.

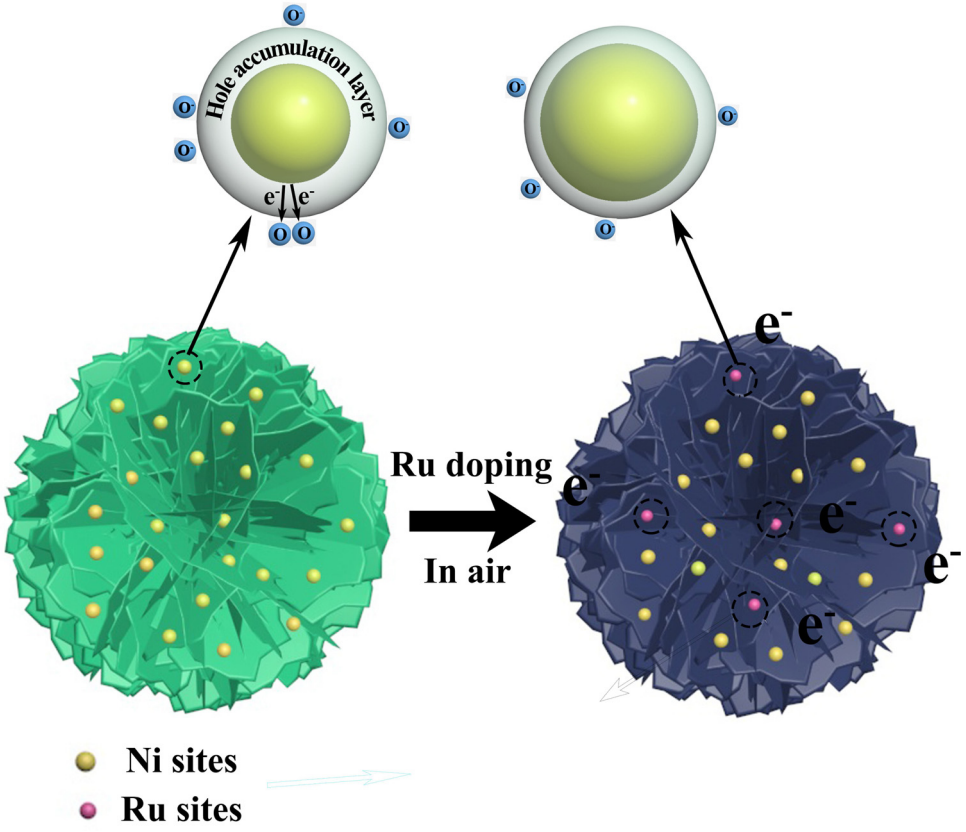

Fig. 10. Schematic illustration of sensing mechanism.

Table 2
The percentages of three different O 1s components in the five samples.

sample	Lattice oxygen O_L(%)	Defect oxygen O_D(%)	Chemisorbed oxygen O_C(%)	Sum of O_D and O_C (%)
Pure NiO	63.8	20.3	15.9	36.2
0.1 at% Ru	51.8	25.2	23	48.2
0.5 at% Ru	20.8	52.1	27.1	79.2
1.0 at% Ru	30	42.6	27.4	70
1.5 at% Ru	38.2	45.7	16.1	61.8

enhanced gas response can be attributed to the increase of relative percentages of O_D and O_C, resistance of the sensing body through Ru doping. The property of high stability to humidity changes can be ascribed to the defect-rich surface of the sensing body after Ru doping. By the way, the catalytic effect of Ru has the contribution to both the gas enhancement and the independence on humidity. This work indicates that Ru doping can not only enhance the gas response but also reduce the impact of humidity on performance of NiO-based gas sensors through proper synthetic process.

CRediT authorship contribution statement

Man Yang: Conceptualization, Methodology, Writing - original

Table 3
Comparison of acetone sensing performance between gas sensor in this work and previously reported results.

Sensing Materials	T (°C)	Conc. (ppm) &RH (%)	RH (%) test range	R_g/R_a or R_a/R_g	$S_{H\%\ RH}/S_{L\%\ RH}$	Improved Ratio	Ref.
Pd-ZnO NSs	340	100&-	–	70	–	1.87	[43]
Al-doped ZnO NPS	450	10&Dry	Dry-90	245	0.10($S_{90\%\ RH}/S_{Dry}$)	19	[44]
23 wt% C-doped WO_3	300	2&18	18-90	7.5	0.41($S_{90\%\ RH}/S_{18\%\ RH}$)	–	[45]
1 wt% Ru-loaded WO_3	300	1.5&-	–	7.3	–	5	[46]
NiO/SnO_2 hierarchical structures	300	50&-	–	20.18	–	3.3	[47]
0.25 at% Au/In-$ZnSnO_3$	200	50&23	23-75	19.3	0.68($S_{75\%\ RH}/S_{23\%\ RH}$)	2	[48]
2 at% Sb-doped In_2O_3	240	50&-	–	64	–	5	[49]
Fe_3O_4-ZnO hierarchical structures	475	50&-	–	47	–	2.4	[50]
10 at% Si-doped WO_3	400	0.6&Dry	Dry-90	4.6	0.33($S_{90\%RH}/S_{Dry}$)	–	[51]
0.5 at% Ru-doped NiO	200	100&50	15-90	12.58	0.97($S_{90\%\ RH}/S_{15\%\ RH}$)	9.6	This work

$S_{H\%\ RH}/S_{L\%\ RH}$: the ratio of gas responses tested under a high humidity condition and in a low humidity condition.
Improved ratio: the ratio of gas responses between the modified gas sensor and untreated sensor under the same condition.

draft, Writing - review & editing. **Jingyuan Lu:** Conceptualization, Methodology, Visualization. **Xi Wang:** Software, Investigation. **Hong Zhang:** Investigation. **Fang Chen:** Formal analysis. **Jianbo Sun:** Investigation. **Jiaqi Yang:** Investigation. **Yanfeng Sun:** Conceptualization, Methodology, Writing - review & editing, Project administration, Funding acquisition. **Geyu Lu:** Conceptualization, Writing - review & editing, Project administration, Supervision, Funding acquisition.

Declaration of Competing Interest

The authors declare that they have no known competing financial interests or personal relationships that could have appeared to influence the work reported in this paper.

Acknowledgements

This work was supported by National Nature Science Foundation of China (Nos. 61573164, 61520106003, 61831011, 61327804).

References

[1] I.D. Kim, A. Rothschild, H.L. Tuller, Advances and new directions in gas-sensing devices, Acta Mater. 61 (2013) 974–1000.
[2] G. Korotcenkov, Metal oxides for solid-state gas sensors: what determines our choice, Mater. Sci. Eng. B 139 (2007) 1–23.
[3] A. Dey, Semiconductor metal oxide gas sensors: a review, Mater. Sci. Eng. B 229 (2018) 206–217.
[4] T.T. Wang, S.Y. Ma, L. Cheng, X.L. Xu, J. Luo, X.H. Jiang, W.Q. Li, W.X. Jin, X.X. Sun, Performance of 3D SnO_2 microstructure with porous nanosheets for acetic acid sensing, Mater. Lett. 142 (2015) 141–144.
[5] W. Liu, Y.L. Xie, T.X. Chen, Q.X. Lu, S.U. Rehman, L. Zhu, Rationally designed mesoporous In_2O_3 nanofibers functionalized Pt catalysts for high-performance acetone gas sensors, Sens. Actuators B 298 (2019) 126871.
[6] Y.Y. Li, H. Yu, Y. yang, T.T. Dong, Fabrication of 3D ordered mesoporous ball-flower structures ZnO material with the excellent gas sensitive property, Sens. Actuators B 300 (2019) 127050.
[7] X. Wang, F. Chen, M. Yang, L.L. Guo, N. Xie, X.Y. Kou, Y. Song, Q.J. Wang, Y.F. Sun, G.Y. Lu, Dispersed WO_3 nanoparticles with porous nanostructure for ultrafast toluene sensing, Sens. Actuators B 289 (2019) 195–206.
[8] J. Yang, Y. Ren, Y.K. Yuan, H. Zhao, Y. Wang, L. Wang, M.Z. Wang, J.F. Liu, C.J. Pei, B. Liu, H.Q. Yang, Enhanced response of hydrogenated Fe_2O_3 nanostructured materials to volatile organic compound vapors and gas sensing mechanism, J. Colloid Interface Sci. 806 (2019) 705–716.
[9] M.S. Yao, L.A. Cao, G.L. Hou, M.L. Cao, J.W. Xiu, C.H. Fang, F.L. Yuan, Y.F. Chen, Gold–tin co-sensitized ZnO layered porous nanocrystals: enhanced responses and anti-humidity, J. Mater. Chem. C 7 (2017) 20273–20280.
[10] Q. Qi, Y.C. Zou, M.H. Fan, Y.P. Liu, S. Gao, P.P. Wang, Y. He, D.J. Wang, G.D. Li, Trimethylamine sensors with enhanced anti-humidity ability fabricated from $La_{0.7}Sr_{0.3}FeO_3$ coated In_2O_3–SnO_2 composite nanofibers, Sens. Actuators B 203 (2014) 111–117.
[11] H.R. Kim, A. Haensch, I.D. Kim, N. Barsan, U. Weimar, J.H. Lee, The role of NiO doping in reducing the impact of humidity on the performance of SnO_2-based gas sensors: synthesis strategies, and phenomenological and spectroscopic studies, Adv. Funct. Mater. 21 (2011) 4456–4463.
[12] H.J. Kim, J.H. Lee, Highly sensitive and selective gas sensors using p-type oxide semiconductors: overview, Sens. Actuators B 192 (2014) 607–627.
[13] M. Hübner, C.E. Simion, A. Tomescu-Stănoiu, S. Pokhrel, N. Bârsan, U. Weimar, Influence of humidity on CO sensing with p-type CuO thick film gas sensors, Sens. Actuators B 153 (2011) 347–353.
[14] X. Cao, Y.J. Xu, N. Wang, Facile synthesis of NiO nanoflowers and their electrocatalytic performance, J. Colloid Interface Sci. 153 (2011) 434–438.
[15] J. Ma, J. Yang, L. Jiao, Y. Mao, T. Wang, X. Duan, J. Lian, W. Zheng, NiO nanomaterials: controlled fabrication, formation mechanism and the application in lithium-ion battery, CrystEngComm 14 (2012) 453–459.
[16] J.W. Lang, L.B. Kong, W.J. Wu, Y.C. Luo, L. Kang, Facile approach to prepare loose-packed NiO nano-flakes materials for supercapacitors, Chem. Commun. (Camb) (2008) 4213–4215.
[17] Y. Cui, C. Wang, S. Wu, G. Liu, F. Zhang, T. Wang, Lotus-root-like NiO nanosheets and flower-like NiO microspheres: synthesis and magnetic properties, Crystengcomm 13 (2011).
[18] Y. Du, W. Wang, X. Li, J. Zhao, J. Ma, Y. Liu, G. Lu, Preparation of NiO nanoparticles in microemulsion and its gas sensing performance, Mater. Lett. 68 (2012) 168–170.
[19] B. Liu, H. Yang, H. Zhao, L. An, L. Zhang, R. Shi, L. Wang, L. Bao, Y. Chen, Synthesis and enhanced gas-sensing properties of ultralong NiO nanowires assembled with NiO nanocrystals, Sens. Actuators B 156 (2011) 251–262.
[20] R. Lontio Fomekong, D. Lahemac, M. Debliquy, V. Duponte, J. Lambi Ngoluia, A. Delcorteb, Co-precipitation synthesis by malonate route, structural characterization and gas sensing properties of Zn-doped NiO, Mater. Today Proc. 3 (2016) 586–591.
[21] S.R. Gawali, V.L. Patil, V.G. Deonikar, S.S. Patil, D.R. Patil, P.S. Patil, J. Pant, Ce doped NiO nanoparticles as selective NO_2 gas sensor, J. Phys. Chem. Solids 114 (2018) 28–35.
[22] M. Ben Amor, A. Boukhachem, A. Labidi, K. Boubaker, M. Amlouk, Physical investigations on Cd doped NiO thin films along with ethanol sensing at relatively low temperature, J. Alloys. Compd. 693 (2017) 490–499.
[23] B.Y. Kim, J.W. Yoon, J.K. Kim, Y.C. Kang, J.H. Lee, Dual role of multiroom-structured Sn-doped NiO microspheres for ultrasensitive and highly selective detection of xylene, ACS Appl. Mater. Interfaces 10 (2018) 16605–16612.
[24] M.U. Haq, Z.Y. Zhang, Z. Wen, S. Khan, S.U. Din, N. Rahman, L.P. Zhu, Humidity sensor based on mesoporous Al-doped NiO ultralong nanowires with enhanced ethanol sensing performance, J. Mater. Sci.-Mater. Electron 30 (2019) 7121–7134.
[25] L. Zhu, W. Zeng, J.D. Yang, Y.Q. Li, Unique hierarchical Ce-doped NiO microflowers with enhanced gas sensing performance, Mater. Lett. 251 (2019) 61–64.
[26] S.H. Lu, X.F. Hu, H. Zheng, J.W. Qiu, R.B. Tian, W.J. Quan, X.J. Min, P. Ji, Y.W. Hu, S.S. Cheng, W. Du, X.Q. Chen, B.L. Cui, X.R. Wang, W. Zhang, Highly selective, ppb-level xylene gas detection by Sn^{2+}-doped NiO flower-like microspheres prepared by a one-step hydrothermal method, Sensors 19 (2019) 2958.
[27] W.N. Shang, D.T. Wang, B.X. Zhang, C.J. Jiang, F.D. Qu, M.H. Yang, Aliovalent Fe (III)-doped NiO microspheres for enhanced butanol gas sensing properties, R. Soc. Chem. 47 (2018) 15181–15188.
[28] R.L. Fomekong, H.M. Tedjieukeng Kamta, J.N. Lambi, D. Lahem, P. Eloy, M. Debliquy, A. Delcorte, A sub-ppm level formaldehyde gas sensor based on Zn-doped NiO prepared by a co-precipitation route, J. Alloys. Compd. 731 (2018) 1188–1196.
[29] H.Y. Gao, Q. Yu, S.F. Zhang, T.S. Wang, P. Sun, H.Y. Lu, F.M. Liu, X. Yan, F.M. Liu, X.S. Liang, Y. Gao, G.Y. Lu, Nanosheet-assembled NiO microspheres modifified by Sn^{2+} ions isovalent interstitial doping for xylene gas sensors, Sens. Actuators B 269 (2018) 210–222.
[30] J. Wang, J. Su, H. Chen, X.X. Zou, G.D. Li, Oxygen vacancy-rich, Ru-doped In_2O_3 ultrathin nanosheets for efficient detection of xylene at low temperature, J. Mater. Chem. C 6 (2018) 4156.
[31] M.E. Franke, T.J. Koplin, U. Simon, Metal and metal oxide nanoparticles in chemiresistors: does the nanoscale matter, Small 2 (2006) 36–50.
[32] C. Sui, T. Zhang, Y. Dong, F. Yuan, X. Niu, Y. Zhu, Interaction between Ru and Co_3O_4 for promoted catalytic decomposition of N_2O over the Ru_x-Co_3O_4 catalysts, Mol. Catal. 435 (2017) 174–181.
[33] J. Gaudet, A.C. Tavares, S. Trasatti, D. Guay, Physicochemical characterization of mixed RuO_2-SnO_2 solid solutions, Chem. Mater. 17 (2005) 1570–1579.
[34] C. Wang, T.S. Wang, B.Q. Wang, X. Zhou, X.Y. Cheng, P. Sun, J. Zheng, G.Y. Lu, Design of α-Fe_2O_3 nanorods functionalized tubular NiO nanostructure for discriminating toluene molecules, Sci. Rep. 6 (2016) 26432.
[35] S. Bai, H. Liu, R. Luo, A. Chen, D. Li, SnO_2@Co_3O_4 p–n heterostructures fabricated by electrospinning and mechanism analysis enhanced acetone sensing, RSC Adv. 4 (2014) 62862–62868.
[36] L.L. Wang, H.M. Dou, Z. Lou, T. Zhang, Encapsuled nanoreactors (Au@SnO_2): a new sensing material for chemical sensors, Nanoscale 5 (2013) 2686–2691.
[37] G. Korotcenkov, B.K. Cho, Engineering approaches for the improvement of conductometric gas sensor parameters Part 1. Improvement of sensor sensitivity and selectivity (short survey), Sens. Actuators B 188 (2013) 709–728.
[38] M. Tonezzer, T.T.L. Dang, Q.H. Tran, V.H. Nguyen, S. Iannotta, Selective hydrogen sensor for liquefied petroleum gas steam reforming fuel cell systems, Int. J. Hydrogen Energy 42 (2017) 740–748.
[39] T.H. Kim, S.Y. Jeong, Y.K. Moon, J.H. Lee, Dual-mode gas sensor for ultrasensitive and highly selective detection of xylene and toluene using Nb-doped NiO hollow spheres, Sens. Actuators B 301 (2019) 127–140.
[40] H.Y. Liu, Y.H. He, K. Nagashima, G. Meng, T.T. Dai, B. Tong, Z.H. Deng, S. Wang, N.W. Zhu, T. Yanagida, X.D. Fang, Discrimination of VOCs molecules via extracting concealed features from a temperature-modulated p-type NiO sensor, Sens. Actuators B 293 (2019) 342–349.
[41] M. Tonezzer, D.T.T. Le, T.Q. Huy, S. Iannotta, Dual-selective hydrogen and ethanol sensor for steam reforming systems, Sens. Actuators B 236 (2016) 1011–1019.
[42] A. Rydosz, Sensors for enhanced detection of acetone as a potential tool for non-invasive diabetes monitoring, Sensors 18 (2018) 2298.
[43] Y.H. Xiao, L.Z. Lu, A.Q. Zhang, Y.H. Zhang, L. Sun, L. Huo, F. Li, Highly enhanced acetone sensing performances of porous and single crystalline ZnO nanosheets: high percentage of exposed (100) facets working together with surface modification with Pd nanoparticles, ACS Appl. Mater. Interfaces 4 (2012) 3797–3804.
[44] R. Yoo, A.T. Güntner, Y. Park, H.J. Rim, H.-S. Lee, W. Lee, Sensing of acetone by Al-doped ZnO, Sens. Actuators B 283 (2019) 107–115.
[45] J.Y. Shen, L. Zhang, J. Ren, J.C. Wang, H.C. Yao, Z.J. Li, Highly enhanced acetone sensing performance of porous C-doped WO_3 hollow spheres by carbon spheres astemplates, Sens. Actuators B 239 (2017) 597–607.
[46] Y. Li, Z. Hua, Y. Zeng, Z. Qiu, X. Tian, M. Wang, E. Li, Modified impregnation synthesis of Ru-loaded WO_3 nanoparticles for acetone sensing, Sens. Actuators B 265 (2018) 249–256.
[47] J. Hu, J. Yang, W. Wang, Y. Xue, Y. Sun, P. Li, K. Lian, W. Zhang, L. Chen, J. Shi, Synthesis and gas sensing properties of NiO/SnO_2 herarchical structures toward ppb-level acetone detection, Mater. Res. Bull. 102 (2018) 294–303.
[48] Q. Chen, Y. Wang, M.X. Wang, S.Y. Ma, P.Y. Wang, G.H. Zhang, W.J. Chen, H.Y. Jiao, L.W. Liu, X.L. Xu, Enhanced acetone sensor based on Au functionalized In-doped $ZnSnO_3$ nanofibers synthesized by electrospinning method, J. Colloid Interface Sci. 543 (2019) 285–299.
[49] X. Liu, X. Tian, X. Jiang, L. Jiang, P. Hiu, S. Zhang, X. Sun, X. Yang, R. Cao, X. Xu,

Facile preparation of hierarchical Sb-doped In_2O_3 microstructures for acetone detection, Sens. Actuators B 270 (2018) 304–311.
[50] L.H. Zhang, B. Dong, L. Xu, X. Zhang, J. Chen, X. Sun, H. Xu, T. Zhang, X. Bai, S. Zhang, H.W. Song, Three-dimensional ordered ZnO-Fe_3O_4 inverse opal gas sensors toward trace concentration acetone detection, Sens. Actuators B 252 (2017) 367–374.
[51] M. Righettoni, A. Tricoli, S.E. Pratsinis, Si:WO_3 sensors for highly selective detection of acetone for easy diagnosis of diabetes by breath analysis, Anal. Chem. 82 (2010) 3581–3587.
[52] M.A. Peck, M.A. Langell, Comparison of nanoscaledand bulk NiO structural and environmental characteristics by XRD, XAFS, and XPS, Chem. Mater. 24 (23) (2013) 4483–4490.
[53] H.J. Kim, K.I. Choi, K.M. Kim, C.W. Na, J.He. Lee, Highly sensitive C_2H_5OH sensors using Fe-doped NiO hollow spheres, Sens. Actuators B 171–172 (2012) 1029–1037.
[54] Y.H. Lin, J. Wang, J. Cai, M. Ying, R. Zhao, M. Li, C.-W. Nan, Ferromagnetism and electrical transport in Fe-doped NiO, Phys. Rev. B 73 (2006) 193308.
[55] M. Yang, H. Pu, Q. Zhou, Q. Zhang, Transparent p-type conducting K-doped NiO films deposited by pulsed plasma deposition, Thin Solid Films 520 (2012) 5884–5888.
[56] D. Kohl, Function and applications of gas sensors, J. Phys. D: Appl. Phys. 34 (2001) R125.
[57] J.W. Yoon, H.J. Kim, I.D. Kim, J.H. Lee, Electronic sensitization of the response to C_2H_5OH of p-type NiO nanofibers by Fe doping, Nanotechnology 24 (2013) 444005.
[58] Z. Wang, H. Zhou, D. Han, F. Gu, Electron compensation in p-type 3DOM NiO by Sn doping for enhanced formaldehyde sensing performance, J. Mater. Chem. C 5 (2017) 3254–3263.
[59] J.W. Zhao, C.S. Xie, L. Yang, S.P. Zhang, G.Z. Zhang, Z.M. Cai, Enhanced gas sensing performance of Li-doped ZnO nanoparticle film by the synergistic effect of oxygen interstitials and oxygen vacancies, Appl. Surf. Sci. 330 (2015) 126–133.
[60] S. Huang, T. Wang, Q. Xiao, Effect of Fe doping on the structural and gas sensing properties of ZnO porous microspheres, J. Phys. Chem. Solids 76 (2015) 51–58.
[61] C. Wang, X.B. Cui, J.Y. Liu, X. Zhou, X.Y. Cheng, P. Sun, X.L. Hu, X.W. Li, J. Zheng, G.Y. Lu, Design of superior ethanol gas sensor based on Al-doped NiO nanorod-flowers, ACS Sens. 1 (2016) 131–136.
[62] B.Y. Kim, J.S. Cho, J.W. Yoon, C.W. Na, C.S. Lee, J.H. Ahn, Y.C. Kang, J.H. Lee, Extremely sensitive ethanol sensor using Pt-doped SnO_2 hollow nanospheres prepared by Kirkendall diffusion, Sens. Actuators B 234 (2016) 353–360.
[63] J. Hu, F.Q. Gao, S.B. Sang, P.W. Li, X. Deng, W.D. Zhang, Y. Chen, K. Lian, Optimization of Pd content in ZnO microstructures for high-performance gas detection, J. Mater. Sci. 50 (2015) 1935–1942.
[64] N. Yamazoe, New approaches for improving semiconductor gas sensors, Sens. Actuators B 5 (1991) 7–19.
[65] N. Yamazoe, G. Sakai, K. Shimanoe, Oxide semiconductor gas sensors, Catal. Surv. Asia 7 (2003) 1574–9266.
[66] D. Koziej, N. Barsan, U. Weimar, J. Szuber, K. Shimanoe, N. Yamazoe, Water-oxygen interplay on tin dioxide surface: implication on gas sensing, Chem. Phys. Lett. 410 (2005) 321–323.
[67] V.N. Singh, B.R. Mehta, R.K. Joshi, F.E. Kruis, S.M. Shivaprasad, Enhanced gas sensing properties of In_2O_3: Ag composite nanoparticle layers; electronic interaction, size and surface induced effects, Sens. Actuators B 25 (2007) 482–488.
[68] J.X. Wang, B. Zou, S.P. Ruan, J. Zhao, F.Q. Wu, Synthesis characterization, and gas-sensing property for HCHO of Ag-doped In_2O_3 nanocrystalline powders, Mater. Chem. Phys. 117 (2009) 489–493.

Man Yang: Received her B. Eng. degree from the Electronics Science and Engineering department, Jilin University, China in 2018. She is currently studying for his MS degree in College of Electronic Science and Engineering, Jilin University, China.

Jingyuan Lu: Received his PhD from Sichuan University of China in 2018. His work is the synthesis and characterization of the semiconducting functional materials and gas sensors.

Xi Wang: Entered her MS course from department of Physical Chemistry, Jilin University, China, in 2016. Now, she is studying for her PhD degree, engaged in the synthesis and characterization of the semiconducting functional materials and gas sensors.

Hong Zhang: Obtained her PhD from Jilin University of China in 2008. Presently, she is working as lecturer in Electronics Science and Engineering department of Jilin University. Her current research interests are image processing and sensor technology.

Fang Chen: Received her B. Eng. degree from the Electronics Science and Engineering department, Jilin University, China in 2017. Her work is the synthesis and characterization of the semiconducting functional materials and gas sensors.

Jianbo Sun: Received his Doctor's degree in College of Electronic Science and Engineering at Jilin University in 2012. Now he is an associate professor in The Key Laboratory for Photonic and Electronic Bandgap Materials, Ministry of Education, Harbin Normal University, China. He is interested in the development of functional materials and chemical sensors, especial in the graphene, metal oxide materials, optical excitation device and flexible devices.

Jiaqi Yang: Entered his MS course from department of Inorganic Chemistry, Jilin University, China, in 2019. Now, he is studying for his PhD degree, engaged in the synthesis and characterization of the semiconducting functional materials and gas sensors.

Yanfeng Sun: Obtained his PhD from Jilin University of China in 2007. Presently, he is a professor in Electronics Science and Engineering department of Jilin University. His current research interests are nanoscience and gas sensors.

Geyu Lu: Received the BS degree in electronic sciences in 1985 and the MS degree in 1988 from Jilin University in China and the Dr Eng degree in 1998 from Kyushu University in Japan. Now he is a professor of Jilin University, China. Now, he is interested in the development of functional materials and chemical sensors.